DENTAL MATERIALS 33 (2017) 954–965

Available online at www.sciencedirect.com

ScienceDirect

journal homepage: www.intl.elsevierhealth.com/journals/dema

Long-term stability of an injection-molded zirconia bone-level implant: A testing protocol considering aging kinetics and dynamic fatigue

Benedikt C. Spies[a,*], *Madeleine E. Maass*[a], *Erik Adolfsson*[b], *Valter Sergo*[c], *Tobias Kiemle*[d], *Christoph Berthold*[d], *Elisa Gurian*[c], *Stefano Fornasaro*[c], *Kirstin Vach*[e], *Ralf-Joachim Kohal*[a]

[a] *Department of Prosthetic Dentistry, Center for Dental Medicine, Medical Center - University of Freiburg, Faculty of Medicine, University of Freiburg, Hugstetter Str. 55, 79106 Freiburg, Germany*
[b] *Swerea IVF AB, Argongatan 30, 431 53 Mölndal, Sweden*
[c] *Department of Engineering and Architecture, University of Trieste, Via Alfonso Valerio 6/1, 34127 Trieste, Italy*
[d] *Applied Mineralogy, University of Tuebingen, Wilhelmstr. 56, 72074 Tuebingen, Germany*
[e] *Medical Center — University of Freiburg, Center for Medical Biometry and Medical Informatics, Institute for Medical Biometry and Statistics, Hebelstr. 11, 79104 Freiburg, Germany*

ARTICLE INFO

Article history:
Received 11 April 2017
Accepted 6 June 2017

Keywords:
Zirconia
Ceramics
Dental implant
Crystallography
X-ray diffraction
Scanning electron microscopy
Raman spectroscopy

ABSTRACT

Objective. Separately addressing the fatigue resistance (ISO 14801, evaluation of final product) and aging behavior (ISO 13356, standardized sample) of oral implants made from yttria-stabilized zirconia proved to be insufficient in verifying their long-term stability, since (1) implant processing is known to significantly influence transformation kinetics and (2) aging, up from a certain level, is liable to decrease fatigue resistance. Therefore, the aim of this investigation was to apply a new testing protocol considering environmental conditions adequately inducing aging during dynamic fatigue.

Methods. Zirconia implants were dynamically loaded (10^7 cycles), hydrothermally aged (85°, 60 days) or subjected to both treatments simultaneously. Subsequent, monoclinic intensity ratios (X_m) were obtained by locally resolved X-ray microdiffraction (μ-XRD^2). Transformation propagation was monitored at cross-sections by μ-Raman spectroscopy and scanning electron microscopy (SEM). Finally, implants were statically loaded to fracture. Linear regression models (fracture load) and mixed models (X_m) were used for statistical analyses.

Results. All treatments resulted in increased fracture load ($p \leq 0.005$), indicating the formation of transformation induced compressive stresses around surface defects during all treatment modalities. However, only hydrothermal and combinational treatment were found to increase X_m ($p < 0.001$). No change in X_m was observed for solely dynamically loaded samples ($p \geq 0.524$). Depending on the variable observed, a monoclinic layer thickness of 1–2 μm (SEM) or 6–8 μm (Raman spectroscopy) was measured at surfaces exposed to water during treatments.

* *Corresponding author*. Fax: +49 761 270 49250.
E-mail address: benedikt.spies@uniklinik-freiburg.de (B.C. Spies).
http://dx.doi.org/10.1016/j.dental.2017.06.002

Significance. Hydrothermal aging was successfully induced during dynamic fatigue. Therefore, the presented setup might serve as reference protocol for ensuring pre-clinically long-term reliability of zirconia oral implants.

1. Introduction

Based on well-documented clinical outcome, oral implants made from titanium are a valid treatment option in patients care when replacing missing or deteriorated teeth [1]. For patients opposing metals, oral implants made from polycrystalline zirconium dioxide represent the only nowadays available alternative [2]. Zirconium dioxide (ZrO_2, zirconia) presents the phenomenon of allotropy, characterized by temperature-dependent crystal structures [3]. When stabilizing the tetragonal phase at room temperature, the polymorphous character of zirconia allows for stress-induced phase transformation toughening (PTT) [4]. This involves the transformation of metastable tetragonal crystallites to the monoclinic phase in the crack tip stress field. *T–m* transformation is accompanied by volume expansion and induces compressive stress in the zirconia matrix, acting to resist crack propagation. Yttria-stabilized tetragonal zirconia (Y-TZP) is therefore known as ceramic material with comparatively high fracture toughness and strength [5]. On the other hand, a potentially serious limitation of stabilized zirconia for its application in the oral environment was discovered: Y-TZP is prone to low temperature degradation (LTD; "aging") in presence of water vapor [6]. In contrast to stress-triggered PTT, LTD is defined as spontaneous and progressive *t–m* transformation at low temperatures in the presence of water molecules. Once started, phase transformation continuously progresses from the surface into the volume in a layer-by-layer manner, following a linear time law [7]. Aging can result in intergranular micro-cracking, surface-roughening and, up from a certain level, in reduced strength [8]. Finally, PTT and LTD are based upon the same phenomenon and using Y-TZP for the fabrication of biomedical implants, one might not exploit the advantage of the former without being exposed to the risk of the latter. To date, it is unclear whether LTD is of clinical relevance when using Y-TZP as dental implant material. Given the importance of aging kinetics and fatigue resistance of Y-TZP implants, a testing protocol should account for the specific brittle nature of ceramics and the specific behavior of zirconia in terms of phase transformation [9]. To date, two separate international ISO standards are available: ISO 13356 imposes that a maximum of 25 wt% of monoclinic phase is present in test specimens after an accelerated aging test (5 h at 134 °C in a humid atmosphere with an air pressure of 0.2 MPa) [10], whereas ISO 14801 requires a dynamic loading procedure subjecting the implants to different loads, to finally obtain a fatigue resistance curve [11]. Regrettably, only the latter standard evaluates the "market-ready" product but it misses to provide any environmental condition that induces aging. Several hundred failures of hip prosthesis reported in a short time period might have shown that this can be considered irresponsible [12]. ISO 13356 prescribes the evaluation of test specimens with a simplified geometry (bending bars) and a polished surface. However, complex geometries as well as post-processing steps like micro-roughening to enhance osseointegration are known to significantly compromise the mechanical properties and, even more important, accelerate the aging kinetics [13]. In conclusion, ISO 13356 does not account for the real transformation rate of samples with roughened surface and a non-porous bulk [9]. Even if experimental methods to predict and simulate LTD in a given zirconia ceramic are deemed to be highly accurate [7,14], the impact on reliability of final implant designs in combination with stress-inducing dynamic fatigue has not yet been evaluated. There is no standardized protocol available, allowing to assess the effect of aging and simultaneous dynamic fatigue on the mechanical properties of a given type of implant. For instance, an escalating effect of spontaneous (LTD) and stress-triggered (PTT) *t–m* transformation (*e.g.* when implants are subjected to dynamic load in the humid environment of the oral cavity) might be possible.

Therefore, the purpose of the present investigation was to measure the amount of phase transformation, either induced by applied mechanical stress or spontaneously occurring during a hydrothermal treatment, and evaluate its impact on the fracture strength of a screw-retained zirconia prototype implant produced by ceramic injection-molding. The issue of a potential escalating effect of both phenomena should be addressed.

2. Materials and methods

2.1. *Sequence of experimental procedures*

A total of 32 implants were used for the experiment and divided into four groups of eight samples each. Three groups (hereinafter referred to as "test groups") were subjected to treatments, intended to induce phase transformation: two groups were either mechanically loaded in a chewing-simulator (ZM) or aged by means of a hydrothermal treatment (ZH), whereas the third group underwent both mentioned treatments simultaneously (ZMH). The remaining zirconia group received no treatment (ZN) and served as reference for comparison. Subsequently, phase transformation of all zirconia groups was evaluated by locally resolved X-ray microdiffraction (μ-XRD[2]) at 4 different surface positions per sample (n = 32). Furthermore, a cross-section of one sample per test group was evaluated by Raman spectroscopy and scanning electron microscopy (n = 3). Except for the three implants used for cross-sections, all implants were finally loaded to fracture in a static loading test and statistically analyzed.

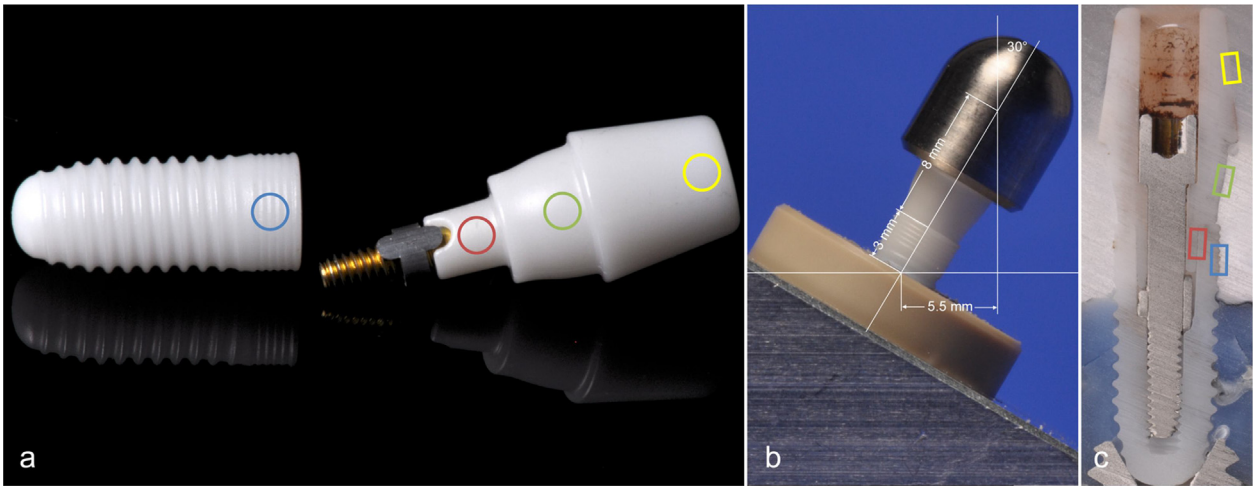

Fig. 1 – The investigational zirconia implants (a) were embedded into PEEK tubes according to ISO 14801 (b). Marked areas at implant/abutment surfaces (a) and at cross-sections (c) visualize the spots for μ-XRD² (a) and Raman/SEM (c) measurements.

2.2. *Investigational zirconia implants*

The zirconia implants were produced by means of ceramic injection-molding (CIM; Prototype development: Cera M GmbH, Wertheim, Germany; Prototype production: Maxon Motor GmbH, Sexau, Germany; Powder: Grade TZ-3Y-E, Tosoh, Tokyo, Japan) and consisted of an endosseous part and a screw-retained abutment (anodized grade 5 titanium screw with anti-rotational protection). The screw-shaped endosseous part was micro-roughened by acid etching, 4.1 mm in diameter, 10.0 mm in length and destined for installation on bone-level (Fig. 1a). The abutment consisted of a concave-shaped transgingival part (gingival height [GH] of 3.0 mm) and a tapered part to be exposed to the oral cavity (5 mm in height). The abutment screws were tightened at 25 Ncm and, additionally, retightened 10 min after the initial torque application to counteract a possible reduction in preload [15].

2.3. *Embedding procedure*

The embedding procedure (according to ISO 14801, Fig. 1b) was already described in detail in a precedent publication [16]. The abutments were equipped with individually machined stainless steel jigs to realize a standardized application of force. For the dynamic and static loading test, all samples were mounted into sample holders at 30° angulation with respect to the vertical axis. For SEM analyses and Raman spectroscopy measurements, samples were embedded in epoxide resin (Araldite 2020, Huntsman Advanced Materials GmbH, Basel, Switzerland) and subsequently cut in half on a precision sectioning saw with a 0,5 mm bronze-bonded diamond sawing blade (Isomet 1000, Buehler GmbH, Duesseldorf, Germany). The embedded and sectioned implants (Fig. 1c) were ground and polished with diamonds and finally polished with a colloidal silica suspension (Struers Rotopol-22 equipped with Struers Rotoforce-4, Struers, Denmark).

2.4. *Dynamic loading test ("mechanical treatment")*

A schematic drawing of the simulation device and its exact setting were described earlier [16]. The implants were subjected to 10 million loading cycles. This aimed to simulate 10–40 years of loading *in vivo*, depending on the underlying data for extrapolation suggesting 240,000 up to 1,000,000 chewing contacts per year [17–20]. A load of 98 N (10 kg) was applied on the highest point to the horizontal of the angulated steel jig. Loading consisted of combined vertical and horizontal forces, representing an approximation to the physiological masticatory cycle of axial pressure and horizontal shear. The loading frequency was set at 2 Hz. During the entire loading period, samples were examined twice a day. Approximately 60 days were necessary to finish the entire 10 million loading cycles of each group.

2.5. *Accelerated aging ("hydrothermal treatment")*

Most of the available studies addressing aging kinetics of zirconia ceramics are based on the *m*-ZrO_2 volume fraction (V_m) measured on the sample surface by XRD after different time and temperature conditions [14] and a subsequent fitting of the gathered sigmoidal curves according to the Mehl–Avrami–Johnson (MAJ) equation [21]

$$V_m(t) = 1 - \exp\left[-(b \cdot t)^n\right], \quad (1)$$

where n is a parameter related to the geometry of the transformation [22] and b a kinetic parameter [14] that follows the Arrhenius law

$$b(T) = b_0 \exp\left(\frac{-Q}{RT}\right), \quad (2)$$

where b_0 is a constant, R (J/mol K) is the universal gas constant, T (K) the absolute aging temperature and Q (J/mol) the activation energy of hydrothermal aging. However, the monoclinic layer thickness (L_m) was found to be better suited for monitor-

ing zirconia's aging kinetics than V_m obtained from the sample surface. Moreover, linear aging kinetics were reported,

$$L_m(t) = S \cdot t \quad (3)$$

questioning the shape of the transformation front in the MAJ kinetic model as mentioned above. The kinetic parameter S (μm/h) can be derived from a plot of L_m as a function of the aging time for different temperatures. Assuming that S follows the Arrhenius equation,

$$S(T) = S_0 \exp\left(\frac{-Q}{RT}\right), \quad (4)$$

the apparent activation energy and the aging kinetics at different temperatures can be derived from a ln(S) vs. 1/T plot. For the present experiment, Q was taken as 104 kJ mol^{-1}, as reported for the same starting powder [23]. From here, it can be calculated that the same L_m can be reached for different time and temperature conditions ((t_1, T_1) and (t_2, T_2)), that verify:

$$t_1 \exp\left(\frac{-Q}{RT_1}\right) = t_2 \exp\left(\frac{-Q}{RT_2}\right), \quad (5)$$

which translates in

$$\frac{t_1}{t_2} = \exp\left(\frac{Q}{R}\left(\frac{1}{T_1} - \frac{1}{T_2}\right)\right), \quad (6)$$

or in

$$\frac{1}{T_2} = \frac{1}{T_1} - \frac{R}{Q}\ln\frac{t_1}{t_2}. \quad (7)$$

Since it was aimed to perform hydrothermal and mechanical treatment simultaneously, t_2 was predefined (t_2 = 60 days, needed for 10 million chewing cycles at 2 Hz with interruptions when examining the implants). Therefore, the environmental temperature during the dynamic loading test had to be calculated so that 60 days correspond to 40 years of aging (t_1 = 14600 days) *in vivo* at 37 °C (T_1=310 K). One can apply Eq. (7) to determine this temperature, resulting in T_2 = 85 °C. Therefore, when loading the ZMH samples, the sample chambers of the chewing simulator were filled with water, set at a temperature 85 °C. The ZH samples were stored in the same chambers without loading contacts.

2.6. μ-XRD^2 measurements

Phase analysis was carried out on different surface positions (implant shoulder, internal abutment-connection, transgingival and oral part of abutment; Fig. 1a) on the tensile side (loading side) of implants and abutments using a Bruker D8 Discover GADDS-microdiffractometer with a Co-sealed tube running at 30 kV/30 mA, a primary monochromator for Kα-radiation and a 500 μm monocapillary optic with a 300 μm pinhole, which results in a beam diameter of 300 μm [24]. The large 2D detector (Bruker VÅNTEC-500) with an angular coverage of 40° in both 2θ and χ was set to a fixed position of 25°, yielding an angle range $15 \leq 2\theta \leq 55°$. The measurement time for each diffractogram was 120 s.

In order to compare the degree of phase transformation after the different treatments, integrated intensity ratios X_m were calculated from the diffractograms according to Garvie and Nicholson [25].

2.7. SEM measurements

The samples were coated with carbon and studied with a field emission scanning electron microscope (Jeol JSM-7800F, Japan).

2.8. Raman spectroscopy measurements

Raman maps were collected on cross-sectioned samples on positions analogous to the μ-XRD^2 analyses (Fig. 1c) in the back-scattering configuration using an InVia Raman microscope (Renishaw plc, Wotton-under-Edge, UK) equipped with a high-power 785 nm near infrared diode laser (Toptica Photonics AG, Germany) delivering 240 mW of laser power to the sample (×50 objective, N.A. 0.9). Under such conditions, the lateral resolution was about 1 μm. A 1800 l/mm grating yielded a spectral resolution of 4 cm^{-1}. A thermoelectrically cooled charge coupled device (CCD) camera was used for detection. The spectrograph was calibrated using the lines of a Ne lamp. Raman data analysis for the tetragonal–monoclinic content was performed with the R software environment for statistical computing using a Partial Least Square subroutine (pls); the results for the phase distribution presented in the Raman maps were also tested against the well-known formula of Clarke and Adar [26]. The agreement between the two methods was in the range of 5% with respect to each other.

2.9. Static loading test

With exception of three samples used for Raman spectroscopy measurements, all samples that survived the dynamic loading procedure were subsequently loaded to fracture using a static material testing machine (Zwick, Z010/TN2S, Ulm, Germany) [16]. Before loading to failure, abutment screws were retightened.

2.10. Fracture analysis

Typical fracture patterns were visualized by scanning electron microscopy (LEO435VP, Zeiss, Oberkochen, Germany) to evaluate crack morphology and identify failure origins. Samples were sputter coated with AuPd for 60 s at 60 mA (SCD050; Leica Microsystems, Wetzlar, Germany).

2.11. Statistical analyses

Implant fracture, either during dynamic loading or subsequently in the static loading test, was declared to be the primary endpoint of the present investigation. Using a sample size of n = 7 per group (one sample per group was used for cross-sections) and an expected standard deviation of approximately 170 N for the fracture load [16] a mean difference of about 12% between the groups could be detected with a power of 80%. For a descriptive analysis of the gathered data (fracture load and X_m), means, medians and standard deviations were computed. For overall analyses, linear regression models were used. For analysis of the fracture load, *t*-tests were used for

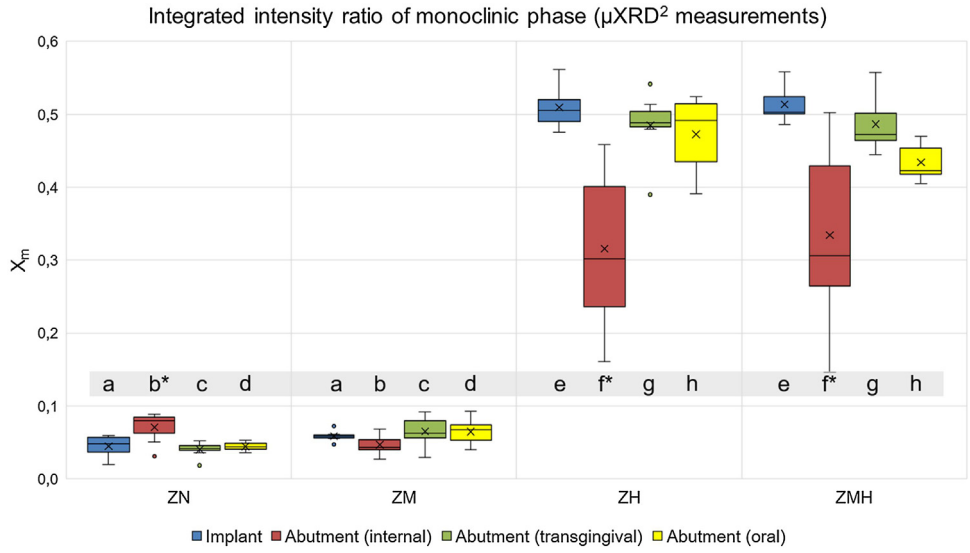

Fig. 2 – Boxplots of the calculated monoclinic phase ratio (X_m) measured by μ-XRD² at 4 different surface positions (implant, internal abutment-connection, transgingival and oral part of abutment) of different groups (ZN, ZM, ZH and ZMH). The results of the statistical analysis (linear mixed models) can be found in the grey shaded area: *Surface position with significantly different X_m compared to other surface positions *within a group*; Corresponding surface positions *across groups* without significantly different X_m were marked with the same letter (a–h).

pairwise comparisons of groups. The method of "Bonferroni" was applied to correct for the multiple testing problem. When analyzing the X_m values, linear mixed models were fitted with random intercepts for each sample. In consequence of four measurement positions per sample the samples were considered as clusters. Multiple pairwise comparisons of different positions within the groups and of corresponding positions across groups were done. Therefore, Scheffé's method was applied to correct for the multiple testing problem. The level of significance was set at $p < 0.05$. The calculations were performed with the statistical software STATA 14 (StataCorp LP, College Station, Texas, USA).

3. Results

3.1. *Dynamic loading test*

The exerted bending moment during the dynamic loading procedure was calculated by multiplication of the applied loading force with the lever arm according to the equation

$$M = y \cdot F = \sin\alpha \cdot l \cdot F \quad (8)$$

where y is the lever arm, α the angle between longitudinal implant axis and loading direction and l the distance from embedding plane to loading center. According to ISO 14801 (Fig. 1b), the dynamically applied load of $F = 98$ N resulted in an exerted bending moment of $M = 53.9$ Ncm. All implants survived the dynamic loading test.

3.2. *μ-XRD² measurements*

Boxplots of the mean integrated intensity ratio X_m of evaluated surface positions are shown in Fig. 2. Within ZN samples, significantly higher X_m values were calculated at the internal abutment-connection ($p < 0.001$). This effect can be attributed to mechanical post-processing after sintering. Within ZH and ZMH samples, significantly reduced X_m values were observed at the internal abutment-connection ($p \leq 0.043$), suggesting a water-shielding effect in that area of some samples. When comparing corresponding surface positions across groups, no significant difference between ZN versus ZM samples and between ZH versus ZMH samples could be calculated ($p \geq 0.154$). Compared to ZN and ZM samples, significantly increased X_m values were found for all corresponding surface positions of ZH and ZMH samples ($p < 0.001$). In brief, only hydrothermal treatment (either alone or in combination with mechanical treatment) was found to significantly increase X_m.

3.3. *Scanning electron microscopy*

A scanning electron microscope (SEM) was used to measure the depth of the monoclinic layer formed during the treatments, which is not directly obtained from the XRD measurements. Fig. 3 shows exemplary images of cross-sectioned samples, where a different contrast was obtained from the grains transformed at the surface compared to mainly unaffected grains below. A damaged monoclinic layer of 1–2 μm is visible at the sample surface of the hydrothermally treated samples (ZH, ZMH), showing intergranular micro-cracks caused by the phase transformation. The solely mechanically treated sample (ZM) shows a significantly reduced monoclinic surface layer of the width of 1–2 grains. One can find several presumably partially transformed grains

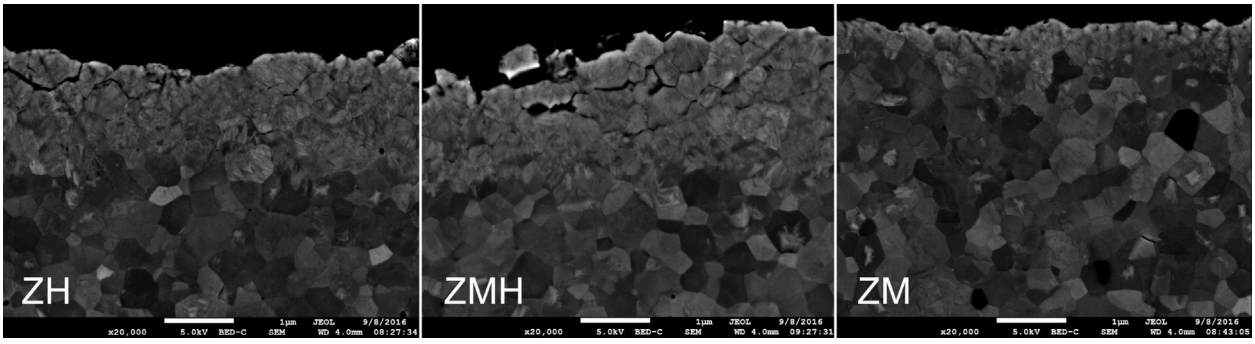

Fig. 3 – Exemplary micrographs of the cross-sectioned ZH (left), ZMH (central) and ZM (right) samples (20000× magnification; location: implant shoulder), showing the martensitic structure of the monoclinic grains and intergranular micro-cracks in the superficial transformed layer and mainly unaffected tetragonal grains below. One can find several presumably partially transformed grains below the most obvious monoclinic layer presenting hints of twinnings/martensitic patterns.

below the most obvious monoclinic layer presenting hints of twinnings/martensitic patterns even well below the obvious, though, irregular, border separating the surface transformed layer from the internal region.

3.4. *Raman spectroscopy measurements*

Fig. 4 shows representative cross-section mappings of three test group samples produced by μ-Raman spectroscopy. Areas of measurement can be seen in Fig. 1c. Monoclinic volume fraction (%) exemplified by Raman spectra of the selected spots is visible from the colored bar at the right side of the maps. The border between the transformed and untransformed zone suggests a penetration depth of the monoclinic phase of approximately 6–8 μm. Again, no distinct phase transformation could be detected at the sample surface when analyzing the mappings of the cross-sectioned ZM sample and at the internal abutment-connection of all samples, in substantial agreement with the findings of the μ-XRD[2] measurements.

3.5. *Static loading test*

Fracture load values can be found in Table 1. Compared to ZN, all treatments of zirconia implants (ZM, ZH, ZMH) resulted in significantly increased fracture load ($p \leq 0.0054$). No statistically significant difference within the test groups (ZM, ZH, ZMH; $p \geq 0.087$) could be observed.

3.6. *Fracture analysis*

Two different fracture patterns could be observed (Fig. 5). All ZH and most of the ZM samples (6/7) fractured horizontally (perpendicular to the implant axis), with crack initiation at the valley of a thread approximately 0.5 mm below the embedding material on the loading side ('fracture pattern 1'; Fig. 5a–d). In contrast, for most of ZMH samples (5/6) fracture origin was observed at both sides of the implant shoulder with a direction of crack propagation along the implant axis ("fracture pattern 2"; Fig. 5e/f). Fracture pattern ($p = 0.018$; $1 > 2$) showed to have significant influence on the exerted load at the time of implant fracture (two-sample *t*-test, Bonferroni-adjusted). This did not change when considering the influence of mechanical loading and hydrothermal aging in a regression analysis.

4. Discussion

The objectives of this study were (1) to evaluate the applied treatment protocol designed to improve the currently available standards for the validation of dental implants made from Y-TZP and (2) to investigate the mechanical long-term reliability of an injection-molded two-piece zirconia implant.

4.1. *Lifetime prediction derived from accelerated aging*

Since it is not feasible to perform long-term aging tests of more than 10 years at body temperature, accelerated tests like the hydrothermal treatment applied in the present investigation are commonly used for extrapolating an estimate of the transformation rate [27]. The underlying aging kinetics and calculated constants were determined at intermediate to high temperatures ranging from 70 to 300 °C and rely on the assumption that the transformation rate follows the same Arrhenius-like trend down to body temperature [28]. However, some authors already assumed faster transformation rates at reduced temperatures than those derived from experiments in the above mentioned temperature range [29,30]. Since the temperature appears in the exponential term of the Arrhenius equation (Eqs. (2), (4)), even a small temperature decrease from 134 °C (as required by ISO 13356) to 85 °C will make the extrapolation to even lower temperatures (body temperature) more acceptable. Furthermore, reduced-temperature experiments need no application of pressure. As already mentioned, the calculated temperature of 85 °C for the hydrothermal treatment in our experiment aimed to simulate 40 years of aging *in situ* in a given 60-day period, assuming an activation energy of 104 kJ mol^{-1}. Nevertheless, the uncertainty of the predicted transformation times derived from an activation energy can be remarkably high, given that the activation energy appears at the exponent of the Arrhenius expression. The performed hydrothermal aging simulation might, however, be regarded a reasonable trade-off, considering both the objection of a potentially faster transformation rate at temperatures below

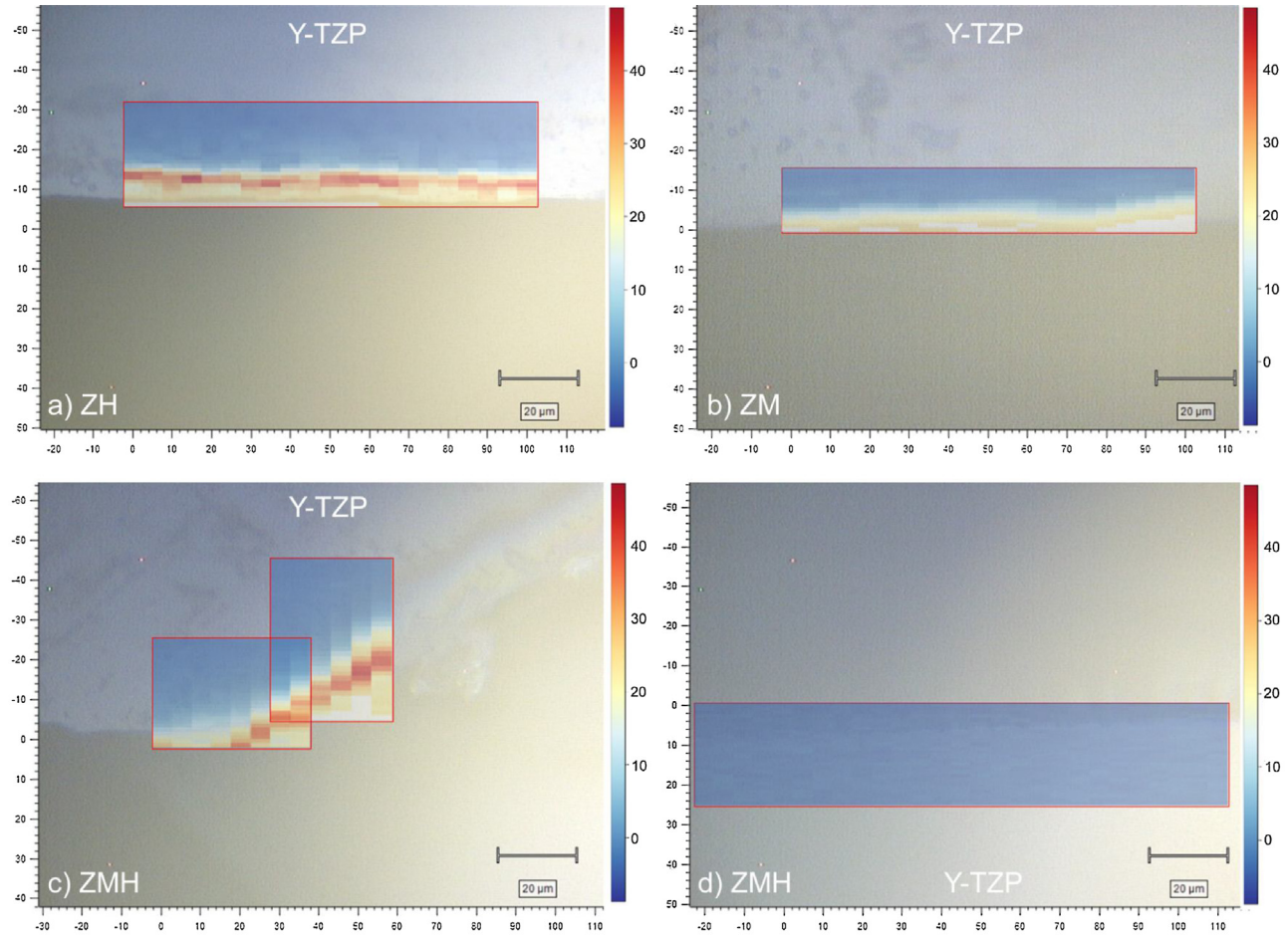

Fig. 4 – Representative quantitative Raman spectroscopy maps of cross-sectioned ZH (a, oral part of abutment), ZM (b, transgingival part of abutment) and ZMH (c, implant shoulder; d, internal abutment-connection) samples (spot size is 1 µm in height and 5 µm in width; *m*-ZrO_2 fraction [%] was calculated with the formula of Clarke and Adar).

the current "standard" of 134 °C and the impossibility of real-time evaluation.

4.2. *Lifetime prediction derived from dynamic loading*

Commercially available chewing simulation devices try to approach the clinical situation by simulating oral parameters such as chewing force (amount, frequency), moisture or lateral jaw motion [20]. Unfortunately, there are no generally accepted values available on how to set the mentioned parameters and standardization appears to be out of reach. Like already mentioned before, there exists no sound clinical data on the number and frequency of chewing contacts performed by humans in their natural environment. Concerning the amount of 10 million loading contacts performed in the present investigation, one can only assume a lifetime estimate in the range of 10–40 years [17,19]. In contrast, there are clinical data available on the exerted bending moment on dental implants *in vivo* during mastication, measured with the help of strain gauges attached to implant abutments. Depending on

Table 1 – Average values for load and bending moment at fracture (load and calculated bending moment at the time of implant fracture in the static loading test) for the different groups. Significantly different values/groups (pairwise comparison, *t*-test, Bonferroni adjusted) are listed in the column "Significance". One ZMH sample was lost.

Group	n					
		mean	SD	mean	SD	
ZN	8	656	74	363	41	ZM, ZH, ZMH
ZM	7	1008	216	555	119	ZN
ZH	7	1134	213	624	117	ZN
ZMH	6	877	36	482	20	ZN

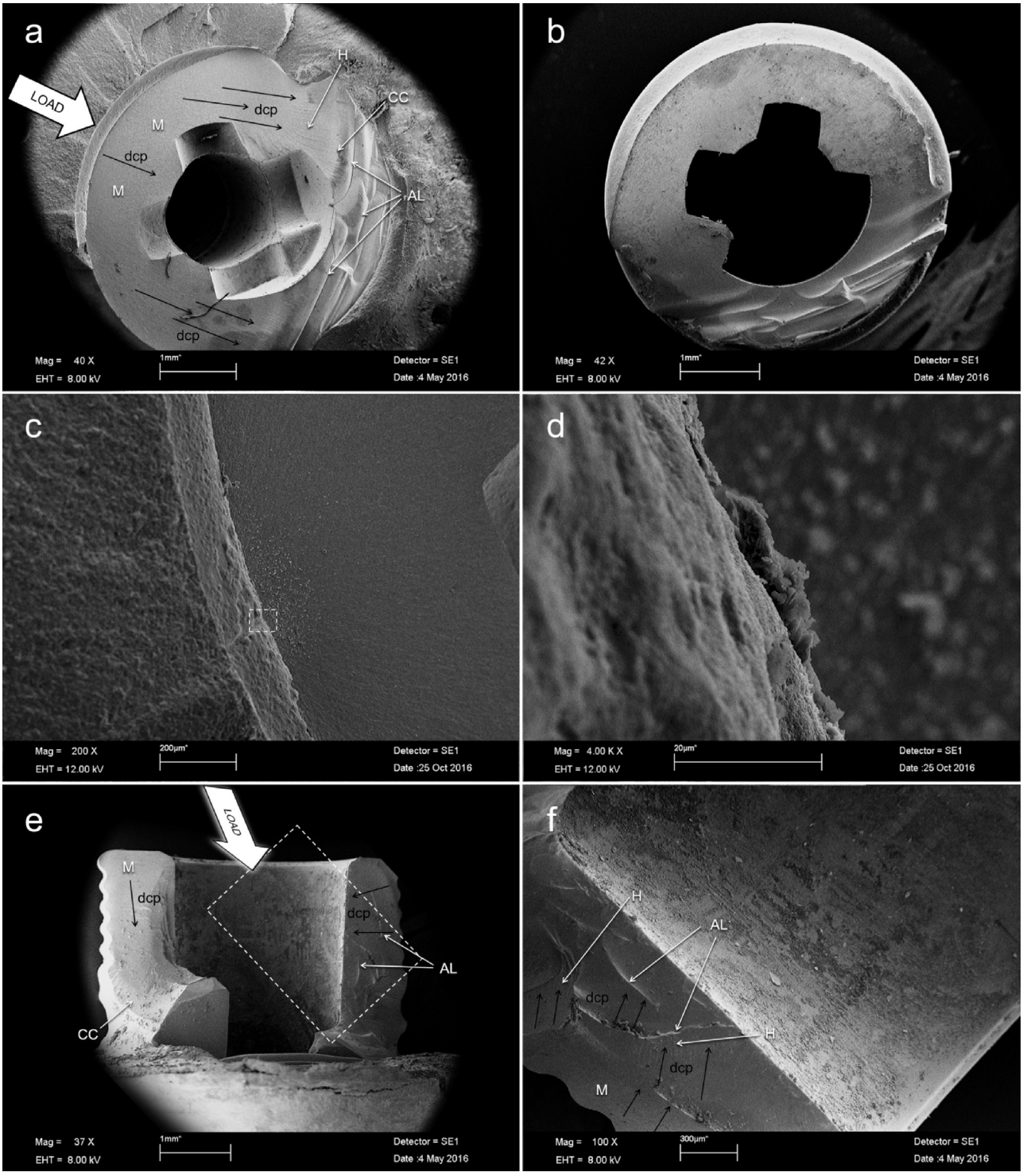

Fig. 5 – SEM image of the two types of observed fracture patterns (a–d: pattern 1; e/f: pattern 2). Fractographic features like a mirror zone ("M"), micro-fine texture hackles ("H"), arrest lines ("AL") and compression curl ("CC") are indicating the direction of crack propagation ("dcp"). Image (b) shows the fragment of (a). Images (c/d) show the fracture origin of (a). The dotted lines in (c/e) contour the magnified sections of (d/f).

the investigation and chosen food, mean bending moments ranging from 5 to 27 Ncm were recorded during physiological chewing activity with peak values up to 95 Ncm [31]. Thus, the dynamically applied load of 54 Ncm in the present investigation was chosen to be twice as high as the highest reported average and might be regarded adequate even when claiming a worst-case scenario.

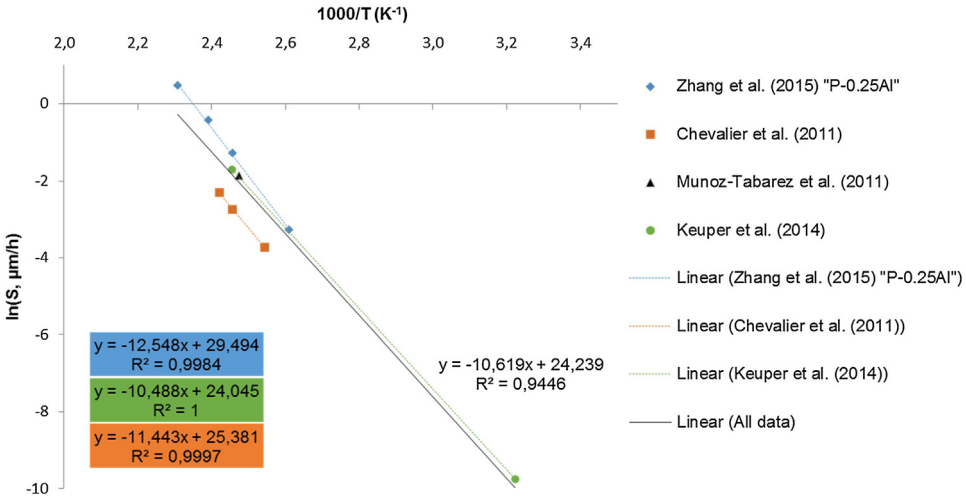

Fig. 6 – Arrhenius plots of ln(S) vs. 1000/T from comparable literature data allowing the extrapolation of aging kinetics to a body temperature of 37 °C and the experimental temperature of 85 °C (Table 2).

4.3. *Suitability of XRD for quantification of monoclinic phase at zirconia implant surfaces*

X-ray diffraction is generally known as the golden standard technique to investigate crystallographic differences like the one of interest in the present investigation (*i.e.*, between the *t*- and *m*-polymorphs of Y-TZP) [28]. As commonly applied in the literature [9], the volume fraction of the monoclinic phase V_m could have been derived after calculating the integrated intensity ratio (X_m) using the formula of Toraya et al. [32]

$$V_m = \frac{P \cdot X_m}{1 + (P-1) \cdot X_m} \quad (9)$$

who experimentally determined P to be 1.311 for the monoclinic–tetragonal ZrO_2 system. Eq. (9) yields an integrated average monoclinic volume percentage over the penetration depth of the X-rays. However, this method for quantification has some major drawbacks for the evaluation of implant surfaces since the calibration curve of Toraya et al. [32] is based on homogeneous mixtures of ZrO_2 powders with various monoclinic–tetragonal ratio. As already mentioned before, phase transformation during the low temperature degradation of zirconia starts on the surface and proceeds linearly into the volume of the ceramic with time [7]. Thus, any measurement spot on the surface of an aged Y-TZP part comprises a surface layer of higher monoclinic content with an underlying tetragonal layer of virtually infinite thickness. Additionally, the XRD patterns of investigated implants and abutments exhibit a pronounced background in the lower angle region (caused by their convex shape). It cannot be ruled out that this leads to distorted results when determining the peak area from which the intensity ratios are calculated. Therefore, under the given conditions, calculation of X_m was only suitable for comparison of different treatment effects, but might not be appropriate for calculation of potentially misleading volume fractions in percent. However, more accurate techniques to evaluate the penetration depth of phase transformation like Raman spectroscopy or SEM imaging require cross-sectioning of the samples, making them useless for subsequent fracture tests. This, however, represented the final measurement of the present work. Therefore, μ-XRD[2] measurements were used for non-destructive data acquisition at different surface positions of all samples to compare and statistically analyze treatment effects.

4.4. *Raman spectroscopy of cross-sectioned implants*

The characteristic maximum inferred information depth of XRD measurements depends on the X-ray wavelength and boundary condition. When the advancing layer front has reached this maximum information depth of the X-ray beam, no information on the further progress can be gathered. Raman measurements at cross-sections are liable to discretize the variation in composition within the diameter of the laser spot. For evaluation of the penetration depth, Raman spectroscopy is, therefore, a far more convenient method [33]. The Raman sampling depth in zirconia ceramics can reach 20 to more than 50 μm, among other variables depending on laser intensity, wavelength and objective lens [34]. Therefore, Raman mappings are not affected by superficial phase transformation that may have occurred during the preparation process of the cross-sections, making this approach more time and cost effective as when compared to focused ion beam (FIB) sectioning with subsequent visualization of the transformation zone by SEM imaging. The observed penetration depth of 6–8 μm after a hydrothermal treatment at 85 °C for 60 days is in accordance with extrapolated data from the nowadays available literature (Fig. 6, Table 2) [23,35]. However, some data (*e.g.* S = 0.5 μm/y at 37 °C) observed for samples aged at body temperature indicate, that the performed aging procedure at 85 °C might not exactly correspond to 40 years of aging at 37 °C [35,36]. Finally, one has to consider that most of the available data were preferably measured on materials where a saturation level was reached in order to have a clear change from the monoclinic to the tetragonal phase [23]. Even if spot res-

Table 2 – Extrapolated data (S [μm/h] at 37/85 °C) gathered from the literature evaluating comparable powder compositions likewise containing 0.25% of alumina (Fig. 11).

	T (°C)	1000/T (1/K)	ln(S)	S (μm/h)	S (μm/year)	μm (60 days)
Zhang et al. [23] "P-0.25Al"	85	2,792	−5,542	0,00392	34,34	5,65
	37	3,224	−10,964	0,00002	0,15	
Chevalier et al. [13]	85	2,792	−6,569	0,00140	12,29	2,02
	37	3,224	−11,514	0,00001	0,09	
Keuper et al. [35]	85	2,792	−5,239	0,00531	46,49	7,64
	37	3,224	−9,771	0,00006	0,50[a]	
All data	85	2,792	−5,412	0,00446	39,11	6,43
	37	3,224	−10,000	0,00005	0,40	

[a] This value was measured at samples aged at body temperature and therefore not extrapolated.

olution was high, the phase change occurred over a distance of around 2 μm (probably due to scattering, the spot size and step length). In the case of the present implant samples, where no saturation was reached at the samples surfaces, it seems to be difficult to precisely determine the penetration depth by solely Raman spectroscopy. Indeed Raman measurements are more suitable for evaluating a sort of *t–m* transition zone rather than a clear-cut penetration depth (which inherently entails the idea of a discrete "quantistic" border).

4.5. *Scanning electron microscopy of cross-sectioned implants*

At a first visual inspection, the monoclinic surface layer observed at the SEM images are thinner (1–2 μm) and monoclinic phase (*t–m* border) could be more clearly distinguished from the tetragonal as when compared to the results gathered by Raman spectroscopy (6–8 μm). Albeit the final word about micro-cracking can only be said by transmission electron microscopy (TEM), evident intergranular micro-cracks were not found in the area close to the *t–m* border (probably due to a lower volume expansion as a result of a none complete transformation) but frequently closer to the surface (larger volume expansion due to a more fully transformed material), which seems to fit quite well with the model presented by Muñoz-Tabares et al. [37], suggesting a "transformation front" of several microns below a "spread" region in which V_m increases dramatically to reach a "saturation" zone directly at the samples surface. SEM imaging might therefore be capable in precisely visualizing saturation and spread, whereas Raman spectroscopy also visualizes a transformation front including single and partially transformed grains, even if this limited transformation can have profound effect on the subsequent aging [38,39]. As we said, measuring the monoclinic layer thickness seems to be a matter of how one defines the "transformation depth": Up to a clearly visible *t–m* border (mostly influencing the samples properties) or up to the last single grains showing signs of transformation.

4.6. *Final static loading to fracture*

As mentioned in the results, all treatments resulted in significantly increased fracture resistance. No significant difference in fracture strength between the treated samples (ZM, ZH, ZMH) could be calculated. However, ZMH samples showed a reduced mean fracture load (877 N), albeit not statistically significant, as when compared to the other treatments (1008/1134 N; Table 1) and 5/6 samples showed a different fracture pattern (Fig. 5e/f). Throughout groups, this fracture pattern was found to be significantly associated with reduced fracture load. Assuming an implant surface with different process related defect sizes or impurities, the largest defects are thought to be responsible for the fracture load of non-treated samples. Increased fracture load of hydrothermally treated zirconia implants is thought to be attributed to the detected transformed layer at the implant surface, inducing an overall compressive stress on the surface tending to close a potential advancing crack at existing surface defects. This phenomenon is liable to cause an increase in strength of the material and was described for the first time nearly 30 years ago [40]. The same effect towards an increased strength was observed by Sanon et al., when loading injection-molded one-piece implants (likewise produced from grade TZ-3Y-E zirconia powder) to failure after different aging times at 134 °C [9]. However, increased strength after an accelerated aging treatment has to be considered specific for the evaluated prototype implant of the present investigation and cannot be taken as general rule for Y-TZP [16]. At some point when the degradation process penetrates deeper into the material, the contribution from the aging may instead cause the strength of the same sample to be decreased [8]. Moreover, mechanical treatment also resulted in increased strength. This might be attributed to stress-induced transformation of only a few single grains around defects where sufficiently high stresses were reached for the phase transformation to occur during the dynamic loading. Compared to a continuous monoclinic surface layer, the transformation of just a few grains (liable to create a local compressive stress) is extremely difficult to detect. The potential fracture initiating defects initially present in the ZN samples may thus, after the mechanical treatment, be subjected to local compressive stress virtually reducing the size of these defects. When the ZM samples were loaded to fracture, a higher load was needed in order to reach the critical tensile stress for the crack to propagate, either due to that the fracture was initiated from another smaller defect or to overcome the local compressive stresses around the originally fracture initiating defects. This can then explain the increase of the fracture load obtained for the ZM samples compared to ZN.

4.7. *Suitability of the experimental setup for lifetime estimation of zirconia dental implants*

As mentioned before, the exact extrapolation of accelerated aging and dynamic loading conditions to finally obtain a lifetime estimation of a zirconia dental implant is still uncertain. It is unclear whether one can assume an Arrhenius-like trend in *t–m* transformation from the experimental temperature down to body temperature and data on *in vivo* chewing frequency are scarce. In contrast to the currently available ISO standards (see above), the presented experimental setup included horizontal shear forces as well as aging inducing conditions during loading and should be liable to verify a long-term mechanical reliability of a zirconia dental implant of at least 10 years, even when assuming the most unfavorable data for extrapolation (1 million chewing cycles per year; $Q > 80\,kJ\,mol^{-1}$, according to Eq. (7)). Since fracture load before and after the applied artificial aging procedure represents the most relevant factor for predicting mechanical reliability, it should be considered the primary outcome and comprise a "safety buffer" of at least 50% as when compared to maximum *in vivo* loading forces on implants or teeth (maximum voluntary contraction or greatest clenching strength measured in clinical trials was reported to be in the range of 350–400 N in the molar region [41–43]). This results in a required fracture load of at least 600 N. For "standard" pre-clinical evaluation of mechanical long-term reliability (as it should be mandatorily required), phase transformation measurements might be considered supplementary for fault tracing or when comparing different materials or processing technologies.

4.8. *Reliability of the evaluated zirconia implant system*

The presented and applied testing protocol aims to verify the reliability of zirconia dental implants and to finally make a recommendation on their safety for clinical application. The mean applied loads in the final fracture test ranged from 656 (ZN) to 1134 N (ZH). Those values are above the before defined benchmark of 600 N. Therefore, in the authors' view, the investigational bone-level zirconia prototype implant proved sufficient mechanical reliability to survive mastication in the oral cavity long-term. Eight titanium implants of comparable design (BEGO Semandos S non-sterile implants, REF 55543; BEGO Implant systems, Bremen, Germany; 4.1 mm in diameter and 10.0 mm in length) revealed a mean fracture load in the same range (846 ± 62 N) when loaded to fracture under identical conditions. However, the investigated zirconia prototype implant represented no final and market-ready product (*e.g.* experimental surface finish). Further changes in feedstock composition, processing, surface preparation or implant design of this prototype need to be re-evaluated by the same procedure.

5. Conclusion

1. In the presented experimental setup, phase transformation was only detectable after hydrothermally induced aging. However, increased fracture load of solely dynamically loaded implants indicated localized stress-induced transformation.
2. Currently applicable ISO standards are not addressing the *in vivo* aging behavior of zirconia oral implants and thereby missing to verify their safety pre-clinically. The presented protocol might serve as a reference for the discussion on how to specify the current standards. A re-worked standard should include the exposure of (1) market-ready implants to (2) lower aging temperatures in order to obtain more reliable data and, furthermore, (3) simultaneous dynamic fatigue at (4) prolonged loading/aging periods as when compared to ISO 13356 and 14801.
3. Strength of the investigated zirconia prototype implant was not reduced by aging, fatigue or simultaneous treatment. However, results are highly specific and other implant systems (even if the zirconia starting powder is the same) might show a complementary effect of simultaneous aging and fatigue (like the present prototype showed in the occurrence of a fracture pattern strongly associated with reduced fracture load).

Disclosure

Investigational implants were provided by the manufacturer (Cera M GmbH).

Acknowledgements

The authors would like to thank Walter Lutz for his help in maintaining the chewing simulator. Ann-Katrin Fetzer and Frieder Lauxmann are acknowledged for performing the XRD measurements. Monica Cristea and Melina Da Silva are acknowledged for sample preparation and microscopy.

REFERENCES

[1] Esposito M, Ardebili Y, Worthington HV. Interventions for replacing missing teeth: different types of dental implants. Cochrane Database Syst Rev 2014;7:CD003815.
[2] Pieralli S, Kohal RJ, Jung RE, Vach K, Spies BC. Clinical outcomes of zirconia dental implants. J Dent Res 2017;96:38–46.
[3] Kisi EH, Howard C. Crystal structures of zirconia phases and their inter-relation. Key Eng Mater 1998;153:1–36.
[4] Gupta TK, Lange FF, Bechtold JH. Effect of stress-induced phase transformation on the properties of polycrystalline zirconia containing metastable tetragonal phase. J Mater Sci 1978;13:1464–70.
[5] Piconi C, Maccauro G. Zirconia as a ceramic biomaterial. Biomaterials 1999;20:1–25.
[6] Kobayashi K, Kuwajima H, Masaki T. Phase change and mechanical properties of ZrO_2–Y_2O_3 solid electrolyte after ageing. Solid State Ion 1981;3:489–93.
[7] Keuper M, Eder K, Berthold C, Nickel KG. Direct evidence for continuous linear kinetics in the low-temperature degradation of Y-TZP. Acta Biomater 2013;9:4826–35.
[8] Kim HT, Han JS, Yang JH, Lee JB, Kim SH. The effect of low temperature aging on the mechanical property & phase stability of Y-TZP ceramics. J Adv Prosthodont 2009;1:113–7.

[9] Sanon C, Chevalier J, Douillard T, Cattani-Lorente M, Scherrer SS, Gremillard L. A new testing protocol for zirconia dental implants. Dent Mater 2015;31:15–25.
[10] ISO 13356. Implants for surgery — ceramic materials based on yttria-stabilized tetragonal zirconia (Y-TZP). 2nd edition ISO 13356:2008(E); 2017. p. 1–20.
[11] ISO 14801:2007. Dentistry – implants – dynamic fatigue test for endosseous dental implants. DIN EN ISO 14801:2008-02; 2017. p. 1–14.
[12] Chevalier J, Gremillard L, Virkar AV, Clarke DR. The tetragonal–monoclinic transformation in zirconia: lessons learned and future trends. J Am Ceram Soc 2009;92:1901–20.
[13] Chevalier J, Loh J, Gremillard L, Meille S, Adolfson E. Low-temperature degradation in zirconia with a porous surface. Acta Biomater 2011;7:2986–93.
[14] Chevalier J, Cales B, Drouin JM. Low-temperature aging of Y-TZP ceramics. J Am Ceram Soc 1999;82:2150–4.
[15] Siamos G, Winkler S, Boberick KG. Relationship between implant preload and screw loosening on implant-supported prostheses. J Oral Implantol 2002;28:67–73.
[16] Spies BC, Nold J, Vach K, Kohal RJ. Two-piece zirconia oral implants withstand masticatory loads: an investigation in the artificial mouth. J Mech Behav Biomed Mater 2016;53:1–10.
[17] DeLong R, Sakaguchi RL, Douglas WH, Pintado MR. The wear of dental amalgam in an artificial mouth: a clinical correlation. Dent Mater 1985;1:238–42.
[18] Sakaguchi RL, Douglas WH, DeLong R, Pintado MR. The wear of a posterior composite in an artificial mouth: a clinical correlation. Dent Mater 1986;2:235–40.
[19] Po JM, Kieser JA, Gallo LM, Tesenyi AJ, Herbison P, Farella M. Time-frequency analysis of chewing activity in the natural environment. J Dent Res 2011;90:1206–10.
[20] Rosentritt M, Behr M, Gebhard R, Handel G. Influence of stress simulation parameters on the fracture strength of all-ceramic fixed-partial dentures. Dent Mater 2006;22:176–82.
[21] Johnson WA, Mehl RF. Reaction kinetics in processes of nucleation and growth. Trans Am Inst Min Metall Eng 1939;135:416–41.
[22] Gremillard L, Chevalier J, Epicier T, Deville S, Fantozzi G. Modeling the aging kinetics of zirconia ceramics. J Eur Ceram Soc 2004;24:3483–9.
[23] Zhang F, Inokoshi M, Vanmeensel K, Van Meerbeek B, Naert I, Vleugels J. Lifetime estimation of zirconia ceramics by linear ageing kinetics. Acta Mater 2015;92:290–8.
[24] Berthold C, Bjeoumikhov A, Brügemann L. Fast XRD2 microdiffraction with focusing X-ray microlenses. Part Part Syst Charact 2009;26:107–11.
[25] Garvie RC, Nicholson PS. Phase analysis in zirconia systems. J Am Ceram Soc 1972;55:303–5.
[26] Clarke DR, Adar F. Measurement of the crystallographically transformed zone produced by fracture in ceramics containing tetragonal zirconia. J Am Ceram Soc 1982;65:284–8.
[27] Sanon C, Chevalier J, Douillard T, Kohal RJ, Coelho PG, Hjerppe J, et al. Low temperature degradation and reliability of one-piece ceramic oral implants with a porous surface. Dent Mater 2013;29:389–97.
[28] Lughi V, Sergo V. Low temperature degradation – aging – of zirconia: a critical review of the relevant aspects in dentistry. Dent Mater 2010;26:807–20.
[29] Sergo V. Room-temperature aging of laminate composites of alumina/3-mol%-yttria-stablilized tetragonal zirconia polycrystals. J Am Ceram Soc 2004;87:247–53.
[30] Lughi V, Clarke DR. Low-temperature transformation kinetics of electron-beam deposited 5 wt.% yttria-stabilized zirconia. Acta Mater 2007;55:2049–55.
[31] Morneburg TR, Pröschel PA. In vivo forces on implants influenced by occlusal scheme and food consistency. Int J Prosthodont 2003;16:481–6.
[32] Toraya H, Yoshimura M, Somiya S. Calibration curve for quantitative analysis of the monoclinic–tetragonal ZrO_2 system by X-ray diffraction. J Am Ceram Soc 1984;67:119–21.
[33] Chevalier J, Gremillard L, Deville S. Low-temperature degradation of zirconia and implications for biomedical implants. Annu Rev Mater Res 2007;37:1–32.
[34] Presser V, Keuper M, Berthold C, Nickel KG. Experimental determination of the Raman sampling depth in zirconia ceramics. Appl Spectrosc 2009;63:1288–92.
[35] Keuper M, Berthold C, Nickel KG. Long-time aging in 3 mol.% yttria-stabilized tetragonal zirconia polycrystals at human body temperature. Acta Biomater 2014;10:951–9.
[36] Dehestani M, Adolfsson E. Phase stability and mechanical properties of zirconia and zirconia composites. Int J Appl Ceram Tech 2013;10:129–41.
[37] Muñoz-Tabares JA, Jiménez-Piqué E, Anglada M. Subsurface evaluation of hydrothermal degradation of zirconia. Acta Mater 2011;59:473–84.
[38] Sergo V, Clarke DR. Deformation bands in ceria-stabilized tetragonal zirconia/alumina: II, stress-induced aging at room temperature. J Am Ceram Soc 1995;78:641–4.
[39] Sergo V, Clarke DR, Pompe W. Deformation bands in ceria-stabilized tetragonal zirconia/alumina: I, measurement of internal stresses. J Am Ceram Soc 1995;78:633–40.
[40] Virkar AV, Huang JL, Cutler RA. Strengthening of oxide ceramics by transformation-induced stress. J Am Ceram Soc 1987;70:164–70.
[41] Imamura Y, Sato Y, Kitagawa N, Uchida K, Osawa T, Omori M, et al. Influence of occlusal loading force on occlusal contacts in natural dentition. J Prosthodont Res 2015;59:113–20.
[42] Hidaka O, Iwasaki M, Saito M, Morimoto T. Influence of clenching intensity on bite force balance, occlusal contact area, and average bite pressure. J Dent Res 1999;78:1336–44.
[43] Kobari H, Yoda N, Chen J, Kawata T, Sasaki K. An in vivo study on load distribution in different implant configurations for supporting fixed partial dentures. Int J Oral Maxillofac Implants 2016;31:1049–57.